Cell Reports
Report

SAP102 Mediates Synaptic Clearance of NMDA Receptors

Bo-Shiun Chen,[1,2,5,*] John A. Gray,[3,5] Antonio Sanz-Clemente,[1] Zhe Wei,[2] Eleanor V. Thomas,[1] Roger A. Nicoll,[3,4] and Katherine W. Roche[1,*]

[1]National Institute of Neurological Disorders and Stroke, National Institutes of Health, Bethesda, MD 20892, USA
[2]Department of Neurology and Program of Developmental Neurobiology, Institute of Molecular Medicine and Genetics, Georgia Health Sciences University, Augusta, GA 30912, USA
[3]Department of Cellular and Molecular Pharmacology
[4]Department of Physiology
University of California, San Francisco, San Francisco, CA 94143, USA
[5]These authors contributed equally to this work
*Correspondence: bochen@georgiahealth.edu (B.-S.C.), rochek@ninds.nih.gov (K.W.R.)
http://dx.doi.org/10.1016/j.celrep.2012.09.024

SUMMARY

Membrane-associated guanylate kinases (MAGUKs) are the major family of scaffolding proteins at the postsynaptic density. The PSD-MAGUK subfamily, which includes PSD-95, PSD-93, SAP97, and SAP102, is well accepted to be primarily involved in the synaptic anchoring of numerous proteins, including N-methyl-D-aspartate receptors (NMDARs). Notably, the synaptic targeting of NMDARs depends on the binding of the PDZ ligand on the GluN2B subunit to MAGUK PDZ domains, as disruption of this interaction dramatically decreases NMDAR surface and synaptic expression. We recently reported a secondary interaction between SAP102 and GluN2B, in addition to the PDZ interaction. Here, we identify two critical residues on GluN2B responsible for the non-PDZ binding to SAP102. Strikingly, either mutation of these critical residues or knockdown of endogenous SAP102 can rescue the defective surface expression and synaptic localization of PDZ binding-deficient GluN2B. These data reveal an unexpected, nonscaffolding role for SAP102 in the synaptic clearance of GluN2B-containing NMDARs.

INTRODUCTION

NMDARs are ionotropic glutamate receptors that play important roles in excitatory neurotransmission, synaptic plasticity, and neuronal development (Lau and Zukin, 2007). Precise regulation of NMDAR trafficking and synaptic localization is essential for these functions. NMDARs are localized at the postsynaptic membrane, and are stabilized through interactions with membrane-associated guanylate kinases (MAGUKs)(Wenthold et al., 2003). PSD-93, PSD-95, SAP97, and SAP102 are collectively known as PSD-MAGUKs and possess three PDZ domains, a Src homology 3 (SH3) domain and an inactive guanylate kinase (GK) domain (Elias and Nicoll, 2007). The PDZ domains bind to the C termini of NMDARs, whereas the SH3 and GK domains interact with cytoskeletal proteins and intracellular signaling complexes. Although PSD-MAGUKs share a common modular structure, each family member possesses a distinct N-terminal domain. The N termini of PSD-95, PSD-93, and SAP97 contain either a pair of palmitoylated cysteines that stabilize them at synapses or an L27 domain capable of multimerization (Schlüter et al., 2006). The N terminus of SAP102, however, is not palmitoylated and does not have an L27 domain and thus has an unknown function. Recently, we found that the N terminus of SAP102 contains a GluN2B-specific NMDAR binding site (Chen et al., 2011).

Functional NMDARs are heterotetramers assembled with two GluN1 subunits and two GluN2 (GluN2A-GluN2D) and/or GluN3 (GluN3A- GluN3B) subunits. The GluN2 subunits have distinct expression patterns with GluN2A and GluN2B being the major GluN2 subunits in the forebrain. The GluN2 content of NMDARs determines their channel properties, as well as their coupling to distinct intracellular signaling cascades (Cull-Candy and Leszkiewicz, 2004). During development, GluN2B is predominantly expressed in immature neurons and the expression of GluN2A gradually increases, leading to a synaptic switch from GluN2B- to primarily GluN2A-containing NMDARs. In mature neurons, GluN2A-containing NMDARs are primarily localized at synapses, whereas GluN2B-containing receptors are still present at synapses, but also enriched at extrasynaptic sites (Li et al., 2002; Stocca and Vicini, 1998; Tovar and Westbrook, 1999). In addition, GluN2B-containing NMDARs undergo more robust endocytosis (Lavezzari et al., 2004; Roche et al., 2001) and have higher surface mobility than GluN2A-containing receptors (Groc et al., 2006). Biochemical studies have shown that GluN2A preferentially binds to PSD-95 and GluN2B preferentially binds to SAP102 (Sans et al., 2000; van Zundert et al., 2004; although, see Al-Hallaq et al., 2007), and it has been proposed that PSD-95 and SAP102 play a role in the subunit-specific regulation of receptor trafficking and localization (van Zundert et al., 2004). Interestingly, SAP102 is not palmitoylated and is highly mobile at the postsynaptic density, similar to GluN2B (Zheng et al., 2010).

GluN2A and GluN2B share an identical PDZ ligand. However, we have recently identified a secondary non-PDZ GluN2B binding site in the N-terminal domain of SAP102, which might allow for preferential binding of SAP102 and GluN2B (Chen et al., 2011). In the present study, we investigated the role of the PDZ-independent interaction of GluN2B with SAP102 in NMDAR trafficking. We identify two amino acids within the GluN2B C terminus (D1391; D1392) that are critical for binding to the SAP102 N-terminal domain.

Mutating the PDZ ligand on GluN2B profoundly reduces surface expression of NMDARs (Chung et al., 2004; Prybylowski et al., 2005) and the activity-dependent phosphorylation of GluN2B within the PDZ ligand by casein kinase 2 (CK2) drives the removal of GluN2B from the synapse (Sanz-Clemente et al., 2010). We now show that disruption of the secondary SAP102 binding site on GluN2B unexpectedly and dramatically rescues the surface and synaptic expression of PDZ binding-deficient GluN2B. Furthermore, RNAi knockdown of SAP102 also rescued the surface and synaptic expression defect of the GluN2B PDZ ligand mutant. Together, our findings reveal an unexpected role for the PDZ-independent interaction between SAP102 and GluN2B in mediating the synaptic clearance of GluN2B-containing NMDARs.

RESULTS

To identify the PDZ-independent SAP102 binding site in GluN2B, we analyzed a series of GluN2B truncations using a yeast two-hybrid assay. We found a region of the GluN2B C terminus (amino acids 1353–1441) that is required for the non-PDZ interaction (Figure 1A), but attempts to delineate this region further were limited by self-activation of the yeast two-hybrid system. We next generated GluN2A-GluN2B chimeras and found that the GluN2A (1304–1400)-GluN2B (1422–1482) chimera (Figure 1A) interacted with the SAP102 N-terminal domain (Figure 1A), suggesting a short region in GluN2B (1422–1441) is critical for the interaction. Surprisingly, however, this region alone did not interact with the N terminus of SAP102. We therefore postulated that the adjacent region of GluN2B (1353–1400) is a key molecular determinant for binding to the SAP102 N-terminal domain, whereas 1422–1441 is simply permissive but cannot interact independently. Consistently, we found that GluN2B (1–1441) and GluN2B (1–1400), but not GluN2B (1–1353), coimmunoprecipitated with SAP102 (Figures 1A and S1). Based on the chimeras, we hypothesized that the critical residues in the GluN2B (1353–1400) segment must be conserved between GluN2A and GluN2B, but that these residues only interact with the SAP102 N terminus when the GluN2B (1422–1441) region is also present. To test this possibility, we made specific amino acid substitutions within GluN2B (1353–1400), which are identical in the analogous region of GluN2A (1304–1400) (Figure 1B). We first targeted several charged residues and found that the GluN2B D1391K and D1392K mutations (Figure 1B), but not D1378K (Figure S1), disrupted the PDZ-independent binding to SAP102. Moreover, the GluN2B D1391K and D1392K (GluN2B DD-KK) double mutant further reduced the interaction (Figure 1B). We also examined the PDZ-independent interaction using a coimmunoprecipitation assay in HEK293 cells expressing GluN1, GluN2B DD-KK or GluN2B DD-KK S1480E, and SAP102. We found that GluN2B DD-KK S1480E showed a 54% reduction in SAP102 binding compared with GluN2B S1480E (Figure 1B), demonstrating that GluN2B D1391 and D1392 are involved in the interaction of GluN2B with the SAP102 N terminus.

Phosphorylation of Ser1480 within the GluN2B PDZ-binding motif by CK2 disrupts the interaction of GluN2B with PSD-95 and SAP102 and decreases surface expression of GluN2B (Chung et al., 2004). However, the role of the PDZ-independent interaction of GluN2B with SAP102 in NMDAR trafficking is not known. Therefore, we used the GluN2B DD-KK double mutant to study whether the PDZ-independent interaction with SAP102 regulates surface expression of GluN2B. We expressed GFP-GluN2B WT or GFP-GluN2B DD-KK in hippocampal neurons and visualized surface-expressed receptors with an anti-GFP antibody. Surface expression of GFP-GluN2B DD-KK was similar to that of GFP-GluN2B WT (Figure 2). We then investigated whether disruption of both the PDZ and PDZ-independent interactions could affect NMDAR trafficking. To this end, we mutated Ser1480 of GluN2B to glutamate to mimic phosphorylation of Ser1480, which disrupts the PDZ binding of GluN2B and examined the surface expression of GFP-GluN2B S1480E and a combined GFP-GluN2B DD-KK S1480E mutant. Consistent with previous reports (Chung et al., 2004), surface expression of GFP-GluN2B S1480E was dramatically reduced compared to WT (Figure 2). Strikingly, surface expression was recovered with GFP-GluN2B DD-KK S1480E and was similar to wild-type GluN2B (Figure 2), demonstrating that DD-KK mutations, which disrupt binding to the SAP102 N terminus, rescue the surface expression defect of GFP-GluN2B S1480E.

Disruption of an endocytic motif (YEKL) near the C terminus of GluN2B that binds to the clathrin adaptor protein complex AP-2 also restores the surface expression of GluN2B that lacks PDZ binding (Prybylowski et al., 2005; Sanz-Clemente et al., 2010) Thus, to determine if the surface expression rescue seen with the GluN2B DD-KK S1480E mutant (Figure 2) is due to decreased AP-2 binding, we used a yeast two-hybrid binding assay to examine the interaction of GluN2B with μ2, the medium chain of AP-2 that binds to the GluN2B YEKL motif (Lavezzari et al., 2003). However, the DD-KK mutations had no effect on GluN2B binding to μ2 (Figure S2), showing that the rescue of the surface expression of GluN2B S1480E is not mediated by the disruption of AP-2 binding.

To physiologically assess the effects of GluN2B mutations on the synaptic localization of NMDARs, we developed a genetic molecular replacement strategy in organotypic hippocampal slice cultures prepared from mice with conditional knockout alleles for both GluN2A and GluN2B ($Grin2a^{fl/fl}Grin2b^{fl/fl}$) (Granger et al., 2011). We have previously shown that neonatal injection of a Cre-expressing virus into the hippocampus of $Grin2a^{fl/fl}Grin2b^{fl/fl}$ mice completely eliminates synaptic NMDAR responses in CA1 pyramidal neurons by postnatal day 14, suggesting that GluN2A and GluN2B account for all synaptic NMDARs in these cells (Gray et al., 2011). Here, hippocampal slice cultures prepared from the $Grin2a^{fl/fl}Grin2b^{fl/fl}$ mice were biolistically transfected with Cre at DIV2-4, and paired whole-cell recordings were obtained from a Cre-expressing and a

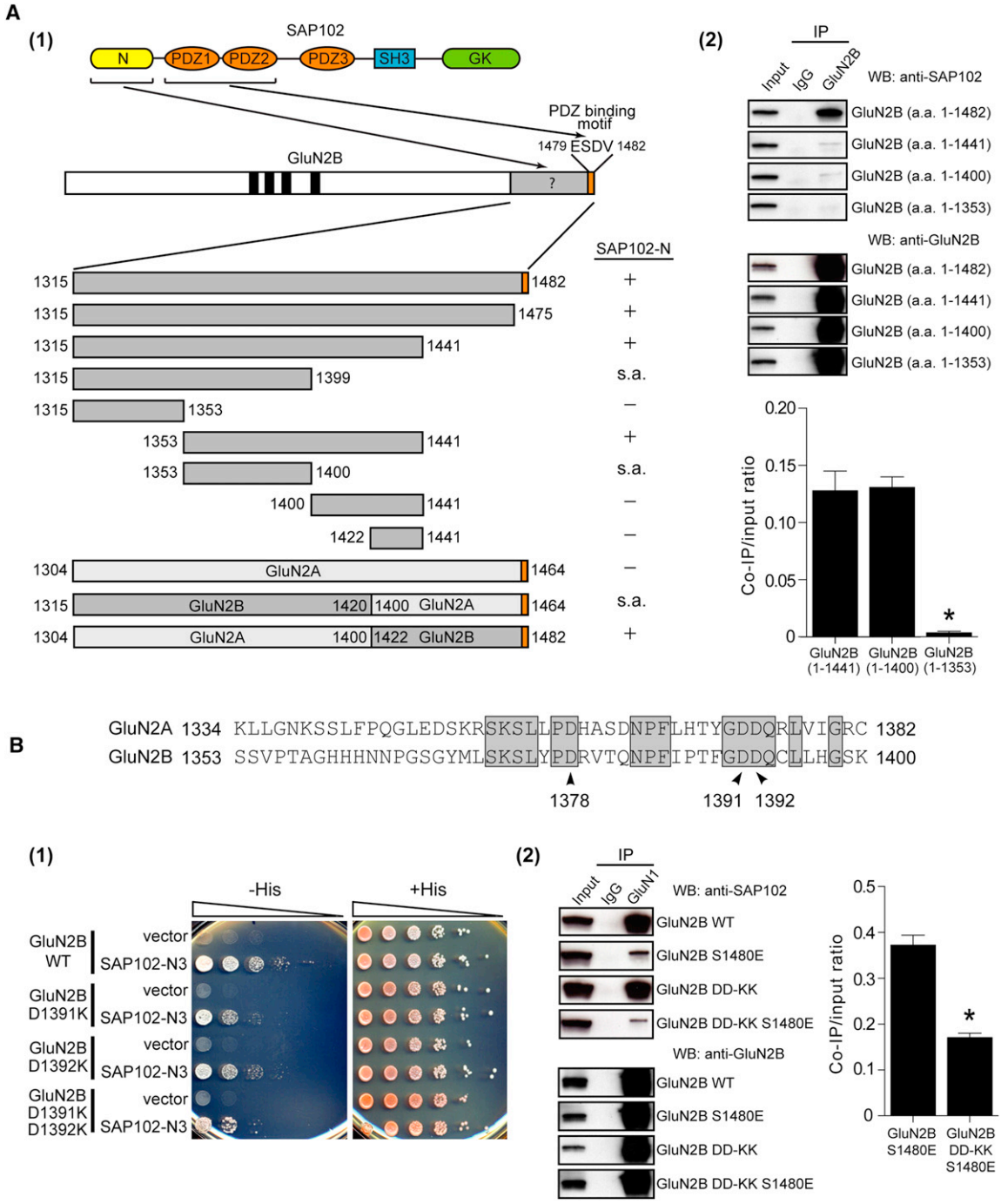

Figure 1. Two Critical Residues in GluN2B Regulate the PDZ-Independent Interaction with SAP102

(A) (1) Schematics of PDZ-dependent and PDZ-independent interactions between GluN2B and SAP102. Various constructs are shown aligned under full-length GluN2B. The interaction of GluN2B constructs with the N-terminal domain of SAP102 are shown, as measured by the yeast two-hybrid binding assay. s.a. indicates there was self activation of the expression construct so the interaction assay could not be performed. (2) HEK293 cells were transfected with GFP-GluN2B (1–1482), GFP-GluN2B (1–1441), GFP-GluN2B (1–1400) or GFP-GluN2B (1–1353), and SAP102. Receptors were immunoprecipitated from cell lysates with anti-GluN2B antibodies or IgG antibodies as a negative control. Immunoprecipitates were resolved by SDS-PAGE and immunoblotted with anti-SAP102 or anti-GluN2B antibodies. Input = 10% of total cell lysate. The data were quantified by measuring co-IP/input SAP102 band intensity ratios using ImageJ software. Data represent means ± SEM (n = 3 independent experiments). See also Figure S1.

(B) An alignment of GluN2A (1334–1382) and GluN2B (1353–1400) are shown. GluN2B D1378, D1391, and D1392 are indicated with arrowheads. The N3 domain of SAP102 (101–148) is the minimum region required for the non-PDZ interaction (Chen et al., 2011). (1) Yeast were cotransformed with LexA-GluN2B, LexA-GluN2B D1391K, LexA-GluN2B D1392K, or LexA-GluN2B D1391K D1392K and Gal4 vector or Gal4-SAP102-N3, and growth was evaluated on appropriate yeast

neighboring control cell at DIV18-24 (Figure 3A). Simultaneous paired dual-cell recordings allow for a rigorous, quantitative study of the postsynaptic effects of the genetic manipulation while controlling for presynaptic inputs. As shown in Figure 3B, 2 weeks of Cre expression reduced the NMDAR-mediated excitatory postsynaptic current (EPSC) by approximately 90% of control cell levels. Longer incubation prior to recording would likely reduce the EPSC further, though slice health becomes limiting. Importantly, the duration of NMDAR-EPSC decays (τ_W) of the small remaining currents were not different from control (Figure 3B), suggesting that this small population of NMDARs is similar in composition to control cells. When Cre was co-expressed with a wild-type GluN2B construct, there was nearly complete recovery (90%) of the NMDAR-EPSC, with the expected lengthening of the decay kinetics from an introduced population of purely GluN2B-containing NMDARs (Figures 3C and 3D).

To examine the role of the PDZ-independent interaction of GluN2B with SAP102 in the synaptic localization of NMDARs, we coexpressed Cre with the GluN2B DD-KK mutant. Consistent with the surface expression studies in dispersed neuronal cultures, the DD-KK mutant had synaptic NMDAR currents similar to wild-type, whereas GluN2B S1480E did not increase synaptic current over Cre alone (Figures 3C and 3D), suggesting a complete exclusion of GluN2B S1480E from synapses. Remarkably, adding the DD-KK mutation to the S1480E mutant completely rescued the synaptic localization of NMDARs (Figures 3C and 3D). Taken together, these results show that the secondary, PDZ-independent, SAP102 binding site on GluN2B precisely regulates the synaptic localization of NMDARs.

We next investigated if SAP102 knockdown can also rescue the surface expression defect of GluN2B S1480E. We generated a small hairpin RNA (shRNA) that efficiently reduced expression of SAP102 in dissociated cortical neurons (Figure S3) and transduced neurons with lentivirus expressing the SAP102 shRNA at DIV5 and expressed FLAG-GluN2B (WT or S1480E) at DIV10. We again observed reduced surface expression for the GluN2B S1480E mutant (Figure 4A). Notably, however, surface expression of GluN2B S1480E was markedly increased upon SAP102 knockdown, whereas there was no significant change in GluN2B WT surface expression (Figure 4A). Using an shRNA against mouse SAP102 (Figure S3), we knocked down SAP102 in the mouse hippocampal slice culture system. Coexpressing mouse SAP102 shRNA with the GluN2B S1480E mutant rescued approximately 50% of the synaptic NMDAR-EPSC (Figures 4B and 4C). This rescue was completely reversed by coexpression of an shRNA-proofed full-length SAP102, but not a SAP102 splice variant lacking the I1 cassette in the N-terminal domain (Figures 4B and 4C) (Chen et al., 2011). Importantly, knockdown of PSD-95 did not rescue the synaptic expression of GluN2B S1480E (Figures 4B, 4C, and S3). Taken together, these results convincingly demonstrate a critical role for the PDZ-independent SAP102 binding site on GluN2B in the synaptic removal of PDZ binding-deficient GluN2B.

DISCUSSION

In this study, we have revealed a mechanism for the subunit-specific regulation of NMDARs. First, we identify two critical residues in the C terminus of GluN2B (DD-KK mutation) responsible for the GluN2B interaction with the SAP102 N terminus. Second, we show that mutation of these two critical residues rescues the surface expression defect of PDZ binding-deficient GluN2B. Third, we find that knocking down SAP102 also rescues the surface expression defect of PDZ binding-deficient GluN2B, providing powerful evidence that the DD-KK mutation on the GluN2B C termini regulates surface expression via specific binding to SAP102. Thus, the PDZ-independent interaction between GluN2B and SAP102 plays an important role in the trafficking and synaptic localization of the GluN2B-containing NMDARs. These findings support a model in which SAP102 acts as an adaptor to regulate the lateral movement of GluN2B-containing NMDARs from the synaptic to extrasynaptic membrane (Figure 4D).

During development, the subunit composition of synaptic NMDARs changes from mainly GluN2B-containing receptors to primarily GluN2A-containing receptors. This subunit switch is activity-dependent and underlies changes in the functional properties of NMDARs including acceleration of the kinetics of NMDAR-mediated EPSCs and increases in the channel open probabilities (Barria and Malinow, 2002; Bellone and Nicoll, 2007; Gray et al., 2011; Philpot et al., 2001; Sanz-Clemente et al., 2010). In addition, NMDARs are rapidly exchanged between synaptic and extrasynaptic sites through lateral diffusion in immature neurons (Tovar and Westbrook, 2002). It is clear that the subunit composition of synaptic NMDARs can undergo rapid and bidirectional switching depending on the pattern of NMDAR activation at neonatal synapses (Bellone and Nicoll, 2007; Matta et al., 2011). However, the molecular mechanisms underlying the differential NMDAR trafficking during development and synaptic plasticity are unclear. It is clear that both phosphorylation, and protein-protein interactions regulate subunit-specific NMDAR trafficking (Chen and Roche, 2007). In this study, we have uncovered a specific mechanism, which regulates the trafficking and synaptic targeting of GluN2B-containing NMDARs.

PSD-MAGUKs act as scaffolding proteins at the postsynaptic density and organize various signal transduction cascades. Each family member has unique properties, but they can functionally compensate for each other (Elias and Nicoll, 2007). The expression of PSD-MAGUKs is differentially regulated during development. For example, SAP102 is expressed early and is dominant for trafficking and anchoring NMDARs at immature synapses (Sans et al., 2003; Washbourne et al., 2004), whereas PSD-95 is expressed later and is involved in maturation and stabilization

selection medium. Results shown are 10-fold serial dilutions of yeast cells. (2) HEK293 cells were transfected with GluN1, SAP102, and GluN2B constructs. Receptors were immunoprecipitated from cell lysates with anti-GluN1 antibodies or IgG antibodies as a negative control. Immunoprecipitates were immunoblotted with anti-SAP102 or anti-GluN2B antibodies. Input = 5% of total cell lysate. The data were quantified by measuring Co-IP/input SAP102 band intensity ratios using ImageJ software. Data represent means ± SEM (n = 3 independent experiments; *$p < 0.01$). See also Figure S1.

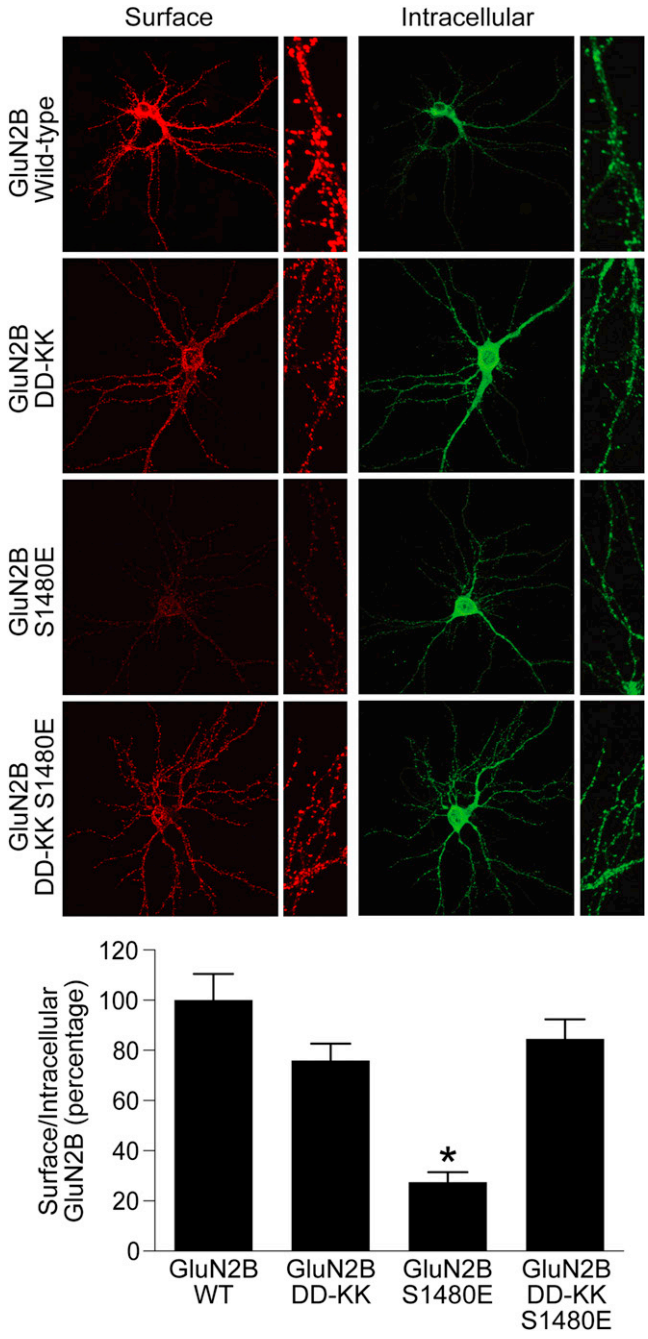

Figure 2. DD-KK Mutations Rescue the Surface Expression of GluN2B S1480E in Neurons

Hippocampal neurons were transfected with GluN2B constructs containing an extracellular GFP tag. Surface staining was performed with anti-GFP and Alexa 568-conjugated (red) anti-rabbit secondary antibodies, followed by fixation and permeabilization, and the internal pool of receptors was labeled with anti-GFP and Alexa 488-conjugated (green) anti-rabbit secondary antibodies. Data represent means ± SEM (n = 27; *p < 0.01) (n = 3 independent experiments). See also Figure S2.

of excitatory synapses (El-Husseini et al., 2000). Although the synaptic function of PSD-95 has been extensively studied, there are relatively few studies on SAP102. Mutations in the human gene encoding SAP102 have been reported to cause mental retardation (Tarpey et al., 2004; Zanni et al., 2010), indicating that SAP102 plays a crucial role in synaptic function. Indeed, mice lacking SAP102 display specific impairments in synaptic plasticity and show cognitive deficits (Cuthbert et al., 2007). However, how SAP102 regulates synaptic function remains elusive. Using fluorescence recovery after photobleaching (FRAP), studies have shown that the majority of SAP102 is highly mobile in dendritic spines and the mobility is rapidly regulated by synaptic activity (Zheng et al., 2010). In contrast, only about a third of PSD-95 is mobile and the mobility is not affected by synaptic activity. Interestingly, studies using single molecule/particle approaches have provided evidence that surface GluN2A-containing NMDARs are much less mobile compared to surface GluN2B-containing receptors (Groc et al., 2006). These results are consistent with earlier studies showing preferential binding between GluN2B and SAP102 (Sans et al., 2000). We have shown that the SAP102 N terminus contains an NMDAR binding site specific for GluN2B (Chen et al., 2011). We now have been able to disrupt this non-PDZ binding by mutating two critical residues in the GluN2B C terminus (DD-KK), although it remains unclear if these residues represent a direct binding site or if the mutations result in disruptive conformational changes. Furthermore, we demonstrate that the specific interaction between GluN2B and SAP102 is important for trafficking of GluN2B-containing NMDARs out of the synapse. Based on our findings, it is likely that the high surface mobility of GluN2B is due to the preferential binding to SAP102, which is extremely mobile in spines.

Glutamate receptor trafficking plays a major role in controlling the number and type of functional receptors during synaptic plasticity. Although endocytosis and exocytosis play a critical role in trafficking of glutamate receptors and synaptic plasticity, lateral diffusion is also important (Cognet et al., 2006; Kennedy and Ehlers, 2006). Endocytic proteins, such as clathrin, AP-2 and dynamin, are localized lateral to the PSD, forming "endocytic zones," allowing efficient endocytosis of receptors that diffuse away from synapses (Rácz et al., 2004). Therefore, it has been suggested that removal of synaptic receptors is a two-step process: uncoupling of receptors from the PSD, followed by lateral movement to an endocytic zone (Rácz et al., 2004). Our studies identify a function of SAP102 in regulating internalization of GluN2B-containing receptors. Our model is consistent with the two-step process of internalization (Figure 4D). First, phosphorylation of GluN2B on S1480 within the PDZ ligand by CK2 disrupts the interaction between synaptic NMDARs and synaptic MAGUKs, such as PSD-95. Second, GluN2B bound to SAP102 through the non-PDZ binding is laterally diffused to the endocytic zone. Extrasynaptic GluN2B is dephosphorylated on Y1472, associates with the AP-2-clathrin endocytic complex, and undergoes endocytosis. Our findings on the subunit-specific interactions between GluN2B and SAP102 provide insight into MAGUK-specific roles in regulating synaptic NMDARs, which were previously unappreciated.

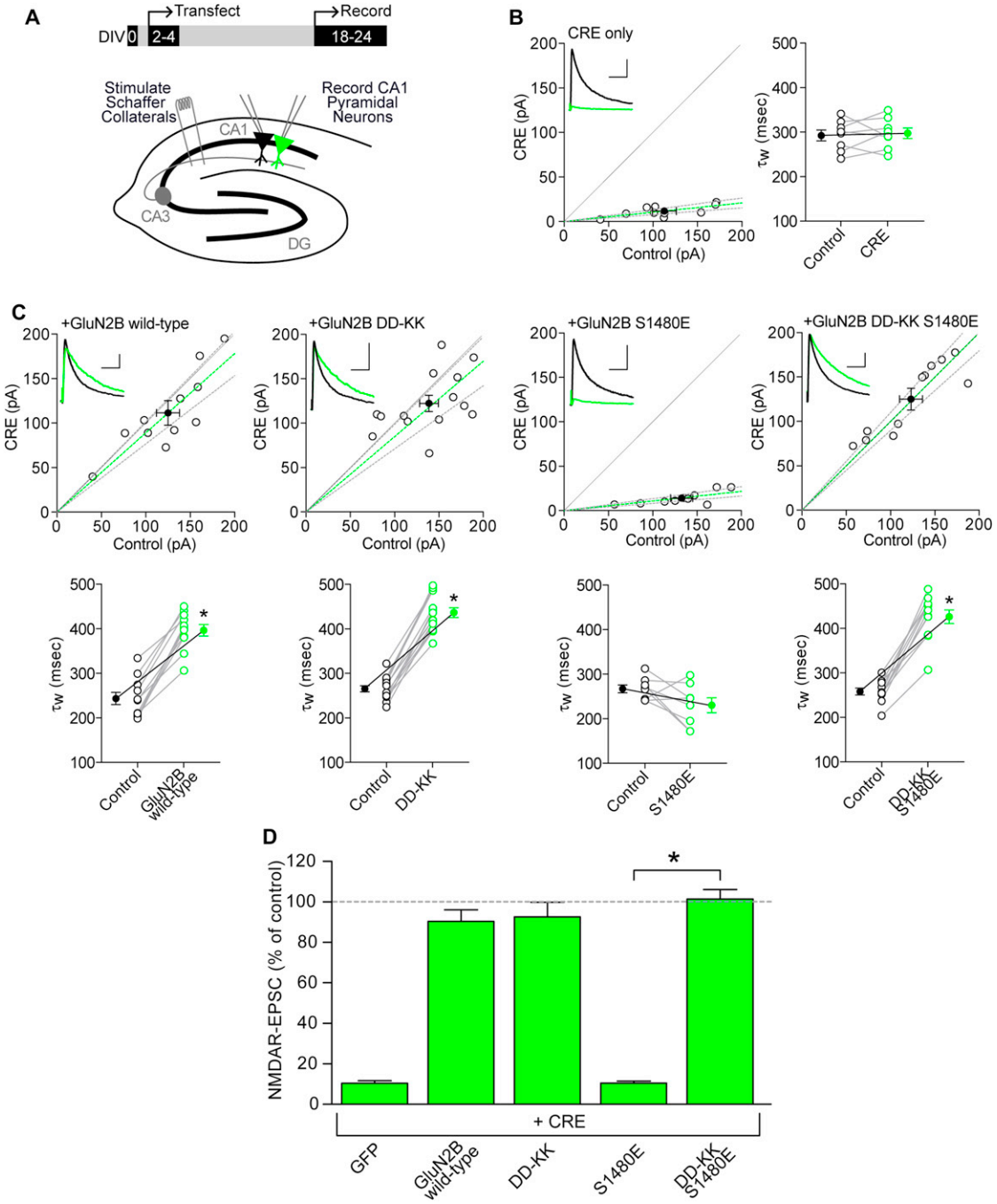

Figure 3. Disruption of Non-PDZ SAP102 Binding Rescues the Synaptic Targeting of PDZ-Deficient GluN2B

(A) Organotypic hippocampal slice cultures were made from P7 *Grin2a*$^{fl/fl}$*Grin2b*$^{fl/fl}$ mice, biolistically transfected at DIV2-4, and paired whole-cell recordings were obtained from Cre-expressing and neighboring CA1 pyramidal neurons at DIV18-24.

(B and C) Scatter plots of peak amplitudes of NMDAR-EPSCs from single pairs (open circles) and mean ± SEM (filled circles) from transfected and control cells. Dashed lines represent linear regression and 95% confidence interval. Sample traces are as follows: control cell, black; transfected cell, green; scale bars represent 100 ms and 40 pA. NMDAR-EPSC decay times expressed in ms as a weighted tau (τ_w) from paired transfected and control cells. (B) Transfection with Cre alone. (C) Cotransfection of Cre with wild-type GluN2B, GluN2B DD-KK, GluN2B S1480E, or the double GluN2B mutant DD-KK S1480E. Decay kinetics were analyzed by a paired Student's t test, *$p < 0.0001$.

(D) Summary graph of data. Bars represent the mean ± SEM of the ratios of transfected to control cells from each pair, expressed as percentages. Data were analyzed by the Mann-Whitney U test, *$p < 0.0001$ compared with GluN2B-S1480E. Actual values for all data can be found in Table S1.

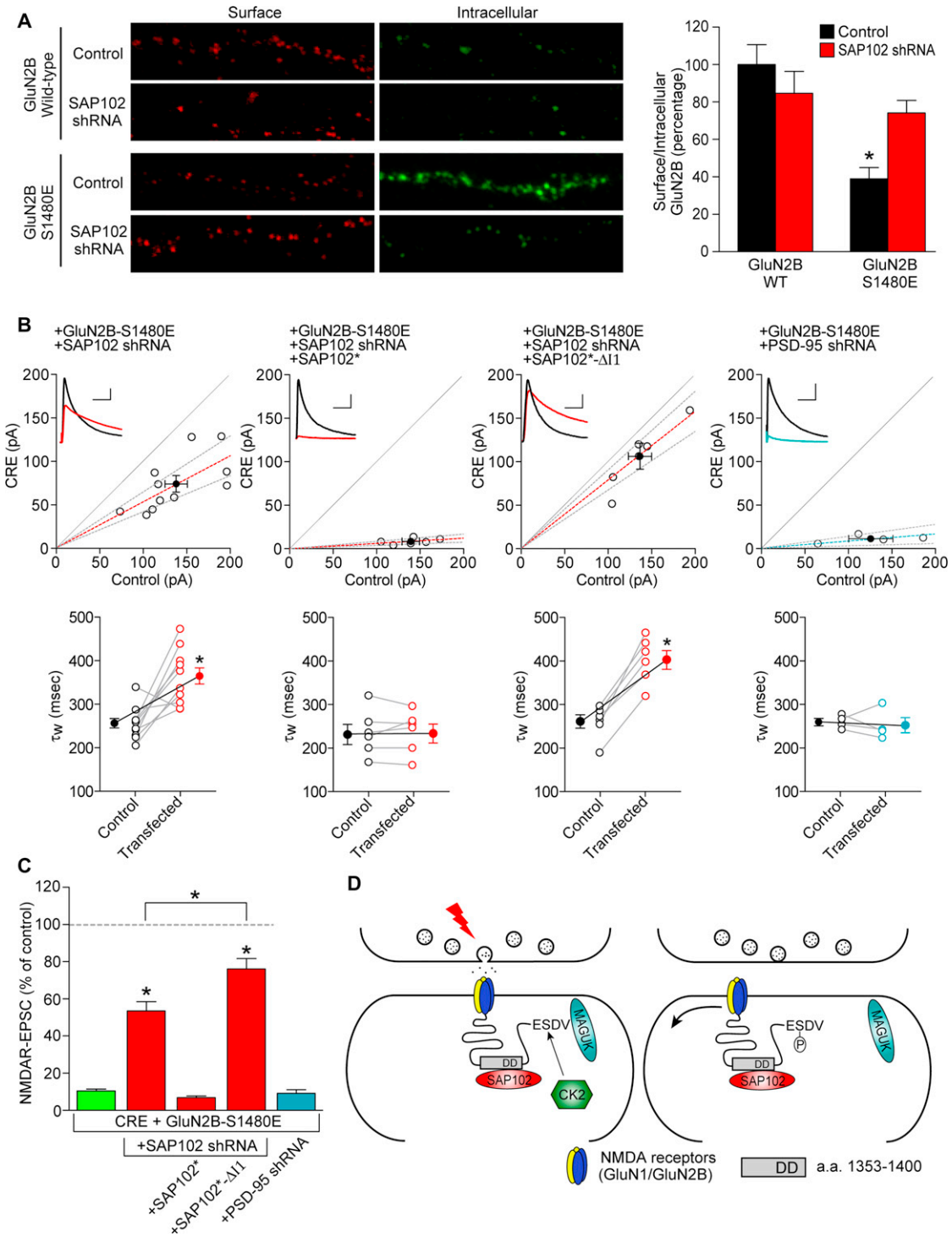

Figure 4. SAP102 Controls GluN2B Synaptic Expression

(A) SAP102 was knocked down in hippocampal cultures by the lentiviral induction of a specific shRNA at DIV5 and Flag-tagged GluN2B constructs (WT or S1480E) were transfected at DIV10. Surface staining was performed with anti-Flag and Alexa 568 secondary antibodies (red) and, after permeabilization, the intracellular pool was labeled with anti-Flag and Alexa 663 secondary antibodies (green). n for GluN2B WT (+/− shRNA) = 26, 26; n for S1480E (+/− shRNA) = 35, 32 (n = 4 independent experiments). Data represent means ± SEM. *p < 0.001. See also Figure S3.

(B) Cotransfection of Cre with GluN2B S1480E, shRNA against mouse SAP102, shRNA-proof SAP102 variants (SAP102*), or shRNA against mouse PSD-95 in hippocampal slice cultures from P7 *Grin2a*$^{fl/fl}$*Grin2b*$^{fl/fl}$ mice. Top, scatter plot of peak amplitudes of NMDAR-EPSCs from single pairs (open circles) and mean ± SEM (filled circles) from transfected and control cells. Dashed lines represent linear regression and 95% confidence interval. Sample traces are as follows: control

EXPERIMENTAL PROCEDURES

The use and care of animals used in this study followed the guidelines of the GHSU, UCSF, and NIH Animal Research Advisory Committees. Yeast two-hybrid assays were performed using L40 yeast strain cotransformed with pBHA and pGAD10 constructs. Immunoprecipitation (IP) was performed at 24 hr after transfection with indicated antibodies. Immunocytochemistry assays were performed in 14 DIV dissociated hippocampal cultures 2 days after transfection with GluN2B constructs. Hippocampi were dissected from P7 *Grin2a*$^{fl/fl}$*Grin2b*$^{fl/fl}$ mice and cotransfected after 2–4 days in culture with pFUGW-Cre:mCherry and either pCAG-GFP or pCAG-GluN2B-IRES-GFP or mutants. Slices were cultured for an additional 14–20 days and dual whole-cell patch-clamp recordings were performed from neighboring CA1 pyramidal cells. NMDAR-EPSCs were recorded at +40 mV in the presence of 10 μM NBQX. Further details available in the Extended Experimental Procedures.

SUPPLEMENTAL INFORMATION

Supplemental Information includes Extended Experimental Procedures, three figures, and one table and can be found with this article online at http://dx.doi.org/10.1016/j.celrep.2012.09.024.

LICENSING INFORMATION

ACKNOWLEDGMENTS

We thank the NINDS sequencing facility and light imaging facility. We also thank Kenji Sakimura (Niigata University) for the Grin2afl/fl and Grin2bfl/fl mice. The research was supported by the NINDS Intramural Research Program (B.-S.C., A.S.-C., E.V.T., and K.W.R.), a NINDS Career Transition Award (E.V.T., Z.W., and B.-S.C.), grants from the NIMH (J.A.G. and R.A.N.). J.A.G. is funded by a NARSAD Young Investigator Award and is the NARSAD Hammerschlag Family Investigator.

Received: March 8, 2012
Revised: June 12, 2012
Accepted: September 14, 2012
Published: October 25, 2012

REFERENCES

Al-Hallaq, R.A., Conrads, T.P., Veenstra, T.D., and Wenthold, R.J. (2007). NMDA di-heteromeric receptor populations and associated proteins in rat hippocampus. J. Neurosci. *27*, 8334–8343.

Barria, A., and Malinow, R. (2002). Subunit-specific NMDA receptor trafficking to synapses. Neuron *35*, 345–353.

Bellone, C., and Nicoll, R.A. (2007). Rapid bidirectional switching of synaptic NMDA receptors. Neuron *55*, 779–785.

Chen, B.S., and Roche, K.W. (2007). Regulation of NMDA receptors by phosphorylation. Neuropharmacology *53*, 362–368.

Chen, B.S., Thomas, E.V., Sanz-Clemente, A., and Roche, K.W. (2011). NMDA receptor-dependent regulation of dendritic spine morphology by SAP102 splice variants. J. Neurosci. *31*, 89–96.

Chung, H.J., Huang, Y.H., Lau, L.F., and Huganir, R.L. (2004). Regulation of the NMDA receptor complex and trafficking by activity-dependent phosphorylation of the NR2B subunit PDZ ligand. J. Neurosci. *24*, 10248–10259.

Cognet, L., Groc, L., Lounis, B., and Choquet, D. (2006). Multiple routes for glutamate receptor trafficking: surface diffusion and membrane traffic cooperate to bring receptors to synapses. Sci. STKE *2006*, pe13.

Cull-Candy, S.G., and Leszkiewicz, D.N. (2004). Role of distinct NMDA receptor subtypes at central synapses. Sci. STKE *2004*, re16.

Cuthbert, P.C., Stanford, L.E., Coba, M.P., Ainge, J.A., Fink, A.E., Opazo, P., Delgado, J.Y., Komiyama, N.H., O'Dell, T.J., and Grant, S.G. (2007). Synapse-associated protein 102/dlgh3 couples the NMDA receptor to specific plasticity pathways and learning strategies. J. Neurosci. *27*, 2673–2682.

El-Husseini, A.E., Schnell, E., Chetkovich, D.M., Nicoll, R.A., and Bredt, D.S. (2000). PSD-95 involvement in maturation of excitatory synapses. Science *290*, 1364–1368.

Elias, G.M., and Nicoll, R.A. (2007). Synaptic trafficking of glutamate receptors by MAGUK scaffolding proteins. Trends Cell Biol. *17*, 343–352.

Granger, A.J., Gray, J.A., Lu, W., and Nicoll, R.A. (2011). Genetic analysis of neuronal ionotropic glutamate receptor subunits. J. Physiol. *589*, 4095–4101.

Gray, J.A., Shi, Y., Usui, H., During, M.J., Sakimura, K., and Nicoll, R.A. (2011). Distinct modes of AMPA receptor suppression at developing synapses by GluN2A and GluN2B: single-cell NMDA receptor subunit deletion in vivo. Neuron *71*, 1085–1101.

Groc, L., Heine, M., Cousins, S.L., Stephenson, F.A., Lounis, B., Cognet, L., and Choquet, D. (2006). NMDA receptor surface mobility depends on NR2A-2B subunits. Proc. Natl. Acad. Sci. USA *103*, 18769–18774.

Kennedy, M.J., and Ehlers, M.D. (2006). Organelles and trafficking machinery for postsynaptic plasticity. Annu. Rev. Neurosci. *29*, 325–362.

Lau, C.G., and Zukin, R.S. (2007). NMDA receptor trafficking in synaptic plasticity and neuropsychiatric disorders. Nat. Rev. Neurosci. *8*, 413–426.

Lavezzari, G., McCallum, J., Lee, R., and Roche, K.W. (2003). Differential binding of the AP-2 adaptor complex and PSD-95 to the C-terminus of the NMDA receptor subunit NR2B regulates surface expression. Neuropharmacology *45*, 729–737.

Lavezzari, G., McCallum, J., Dewey, C.M., and Roche, K.W. (2004). Subunit-specific regulation of NMDA receptor endocytosis. J. Neurosci. *24*, 6383–6391.

Li, B., Chen, N., Luo, T., Otsu, Y., Murphy, T.H., and Raymond, L.A. (2002). Differential regulation of synaptic and extra-synaptic NMDA receptors. Nat. Neurosci. *5*, 833–834.

Matta, J.A., Ashby, M.C., Sanz-Clemente, A., Roche, K.W., and Isaac, J.T. (2011). mGluR5 and NMDA receptors drive the experience- and activity-dependent NMDA receptor NR2B to NR2A subunit switch. Neuron *70*, 339–351.

Philpot, B.D., Sekhar, A.K., Shouval, H.Z., and Bear, M.F. (2001). Visual experience and deprivation bidirectionally modify the composition and function of NMDA receptors in visual cortex. Neuron *29*, 157–169.

cell, black; transfected cell, red; scale bars represent 100 ms and 40 pA. Bottom, NMDAR-EPSC decay times expressed as a weighted tau (τ_w) from paired transfected and control cells. Decay kinetics were analyzed by a paired Student's t test. See also Figure S3.
(C) Bar graph represents mean ± SEM of the ratios of transfected to control cells from each pair, expressed as percentages (GluN2B S1480E is from Figure 3). Data were analyzed by the Mann-Whitney U test, *$p < 0.0001$ compared with GluN2B-S1480E or as indicated. Actual values for all data can be found in Table S1.
(D) Model for the role of SAP102 in regulating GluN2B-containing NMDARs at the synapse. GluN2B-containing NMDARs are stabilized on synaptic membranes through the PDZ interactions with PSD-MAGUKs (PSD-95, PSD-93, SAP97, or SAP102) and non-PDZ interactions with SAP102. Synaptic activity induces GluN2B phosphorylation on S1480 by CK2, which disrupts the PDZ interaction between synaptic NMDARs and MAGUKS at the postsynaptic density. The secondary interaction of GluN2B with the N terminus of SAP102 then facilitates the lateral diffusion of NMDARs to perisynaptic endocytic zones.

Prybylowski, K., Chang, K., Sans, N., Kan, L., Vicini, S., and Wenthold, R.J. (2005). The synaptic localization of NR2B-containing NMDA receptors is controlled by interactions with PDZ proteins and AP-2. Neuron *47*, 845–857.

Rácz, B., Blanpied, T.A., Ehlers, M.D., and Weinberg, R.J. (2004). Lateral organization of endocytic machinery in dendritic spines. Nat. Neurosci. *7*, 917–918.

Roche, K.W., Standley, S., McCallum, J., Dune Ly, C., Ehlers, M.D., and Wenthold, R.J. (2001). Molecular determinants of NMDA receptor internalization. Nat. Neurosci. *4*, 794–802.

Sans, N., Petralia, R.S., Wang, Y.X., Blahos, J., 2nd, Hell, J.W., and Wenthold, R.J. (2000). A developmental change in NMDA receptor-associated proteins at hippocampal synapses. J. Neurosci. *20*, 1260–1271.

Sans, N., Prybylowski, K., Petralia, R.S., Chang, K., Wang, Y.X., Racca, C., Vicini, S., and Wenthold, R.J. (2003). NMDA receptor trafficking through an interaction between PDZ proteins and the exocyst complex. Nat. Cell Biol. *5*, 520–530.

Sanz-Clemente, A., Matta, J.A., Isaac, J.T., and Roche, K.W. (2010). Casein kinase 2 regulates the NR2 subunit composition of synaptic NMDA receptors. Neuron *67*, 984–996.

Schlüter, O.M., Xu, W., and Malenka, R.C. (2006). Alternative N-terminal domains of PSD-95 and SAP97 govern activity-dependent regulation of synaptic AMPA receptor function. Neuron *51*, 99–111.

Stocca, G., and Vicini, S. (1998). Increased contribution of NR2A subunit to synaptic NMDA receptors in developing rat cortical neurons. J. Physiol. *507*, 13–24.

Tarpey, P., Parnau, J., Blow, M., Woffendin, H., Bignell, G., Cox, C., Cox, J., Davies, H., Edkins, S., Holden, S., et al. (2004). Mutations in the DLG3 gene cause nonsyndromic X-linked mental retardation. Am. J. Hum. Genet. *75*, 318–324.

Tovar, K.R., and Westbrook, G.L. (1999). The incorporation of NMDA receptors with a distinct subunit composition at nascent hippocampal synapses in vitro. J. Neurosci. *19*, 4180–4188.

Tovar, K.R., and Westbrook, G.L. (2002). Mobile NMDA receptors at hippocampal synapses. Neuron *34*, 255–264.

van Zundert, B., Yoshii, A., and Constantine-Paton, M. (2004). Receptor compartmentalization and trafficking at glutamate synapses: a developmental proposal. Trends Neurosci. *27*, 428–437.

Washbourne, P., Liu, X.B., Jones, E.G., and McAllister, A.K. (2004). Cycling of NMDA receptors during trafficking in neurons before synapse formation. J. Neurosci. *24*, 8253–8264.

Wenthold, R.J., Prybylowski, K., Standley, S., Sans, N., and Petralia, R.S. (2003). Trafficking of NMDA receptors. Annu. Rev. Pharmacol. Toxicol. *43*, 335–358.

Zanni, G., van Esch, H., Bensalem, A., Saillour, Y., Poirier, K., Castelnau, L., Ropers, H.H., de Brouwer, A.P., Laumonnier, F., Fryns, J.P., and Chelly, J. (2010). A novel mutation in the DLG3 gene encoding the synapse-associated protein 102 (SAP102) causes non-syndromic mental retardation. Neurogenetics *11*, 251–255.

Zheng, C.Y., Petralia, R.S., Wang, Y.X., Kachar, B., and Wenthold, R.J. (2010). SAP102 is a highly mobile MAGUK in spines. J. Neurosci. *30*, 4757–4766.

Cell PRESS
Open ACCESS

EXTENDED EXPERIMENTAL PROCEDURES

DNA Constructs

The pBHA-GluN2B (amino acids 1315 – 1441), pBHA-GluN2B (amino acids 1315 – 1400), pBHA-GluN2B (amino acids 1315 – 1353) constructs, were generated by introducing a stop codon at amino acid 1442, 1401 and 1354 in pBHA-GluN2B (amino acids 1315 – 1475) respectively using site-directed mutagenesis. GluN2B (amino acids 1422 – 1441), GluN2B (amino acids 1400 – 1441), GluN2B (amino acids 1353 – 1400) and GluN2B (amino acids 1353 – 1441) were amplified by PCR using synthetic primers that include flanking EcoRI recognition sequences and subcloned into the LexA fusion vector pBHA. The GluN2B (amino acids 1315 – 1420) - GluN2A (amino acids 1400 – 1464) chimera and the GluN2A (amino acids 1304 – 1400) - GluN2B (amino acids 1422 – 1482) chimera were amplified by PCR using synthetic primers and subcloned into the LexA fusion vector pBHA. GluN2B containing the D1378K, D1391K, or D1392K mutations was generated by site-directed mutagenesis. GFP-GluN2B (amino acids 1 – 1441), GFP-GluN2B (amino acids 1 – 1400) and GFP-GluN2B (amino acids 1 – 1353) were generated by mutating K1442, S1401 and S1354 to a stop codon, respectively using site-directed mutagenesis. shRNA oligonucleotides were inserted into the FHUGW vector. The following shRNA targeting sequences were used for rat SAP102: CCAAGTCCATCGAAGCACT; mouse SAP102: CCAAGTCCATTGAAGCACT, and PSD-95 (identical in mouse and rat): TCACGATCATCGCTCAGTATA (Elias et al., 2006). The shRNA-proofed SAP102 constructs used in mouse hippocampal slice culture are rat clones (Chen et al., 2011).

Yeast Two-Hybrid Assay

The yeast two-hybrid assay was performed as described previously (Chen et al., 2006). Briefly, constructs in the LexA-fusion vector pBHA (*TRP1* plasmid) and the Gal4 activation domain-fusion vector pGAD10 (*LEU2* plasmid) were cotransformed into L40 yeast. After transformation, the yeast were plated in synthetic complete medium lacking leucine and tryptophan (+His). Three independent yeast colonies were selected and assayed for expression of the reporter *HIS3* gene in synthetic complete medium lacking leucine, tryptophan and histidine (−His), demonstrating protein-protein interactions. 3-Aminotriazole (3-AT) (10 mM) was included in the −His medium to reduce or eliminate the background transactivation. All plates were photographed after 3 days of incubation at 30°C.

Immunoprecipitation

Immunoprecipitation was performed as described previously (Cousins and Stephenson, 2012) with some modifications. Briefly, HEK293 cells were transiently transfected with GluN1, GFP-GluN2B and SAP102 using the calcium phosphate method. Cells were harvested 24 hr post–transfection. Transfected HEK293 cells were rinsed twice with PBS and then solubilized for 1 hr at 4°C with 50 mM Tris-citrate, pH 7.4, 240 mM NaCl, 5 mM EDTA, 5 mM EGTA, 1% Triton X-100, protease inhibitor mixture (Roche Applied Science) and phosphatase inhibitor cocktail 1 and 2 (Sigma). The supernatant was collected and centrifuged at 100,000 x g for 20 min at 4°C. For immunoprecipitation, 2 μg of IgG or anti-NR2B antibody (NeuroMab) was used. The supernatant was incubated with antibodies overnight at 4°C. Protein G Dynabeads (Invitrogen) were added, and samples were incubated for 30 min at room temperature and washed three times with solubilization buffer. Precipitates were resolved by SDS-PAGE and transferred to PVDF membrane. The membrane was analyzed by immunoblotting with the relevant antibodies as indicated.

Neuronal Cultures and Immunocytochemistry

Primary hippocampal cultures were prepared from E17-19 Sprague-Dawley rats. Dissociated neurons were plated on poly-D-Lysine-coated coverslips in Neurobasal medium supplemented with B27 and L-glutamine. Hippocampal neurons were transfected at 10-12 days in vitro (DIV) using lipofectamine (lipofectamine 2000, Invitrogen) and immunocytochemistry were performed at DIV14. Briefly, transfected neurons were incubated with polyclonal anti-GFP antibody (Invitrogen) or anti-FLAG antibody (Sigma) for 15 min at room temperature to label surface-expressed protein. The cells were fixed in 4% PFA for 15 min and incubated with Alexa 568-conjugated (red) anti-rabbit secondary antibody (molecular Probes) for 30 min. The cells were permeabilized with 0.25% TX-100, incubated with 10% normal goat serum, and labeled with anti-GFP antibody (Invitrogen) or anti-FLAG antibody (Sigma) for 30 min at room temperature. Following extensive washing, cells were incubated with Alexa 488-conjugated (green; anti-GFP) or Alexa 633-conjugated (green; anti-FLAG) anti-rabbit secondary antibody for 30 min, and mounted with a ProLong Gold Antifade kit (Molecular Probes). Images were collected with a 63X objective on a Zeiss LSM 700 confocal microscope. Series of optical sections collected at intervals of 0.5 μm were used to create maximum projection images. For quantitative analysis, images from three dendrites per neuron from at least three neurons per experiment were collected and quantitated using ImageJ software. At least three independent experiments were performed per condition, and the number of neurons (n) for each condition is indicated in the corresponding figure legend. Measurements were analyzed in Microsoft Excel, and statistical significance was determined by Student's t test.

Electrophysiology in Organotypic Slice Cultures

Double-floxed GluN2AGluN2B (*Grin2a*$^{fl/fl}$*Grin2b*$^{fl/fl}$) mice were generated as previously described (Akashi et al., 2009; Gray et al., 2011; Mishina and Sakimura, 2007), and were housed according to the IACUC guidelines at the University of California, San Francisco. Cultured slices were prepared and transfected as previously described (Schnell et al., 2002). Briefly, hippocampi were dissected from P7 *Grin2a*$^{fl/fl}$*Grin2b*$^{fl/fl}$ mice and biolistically cotransfected after 2-4 days in culture with pFUGW-Cre:mCherry (expressing a nuclear-targeted Cre:mCherry fusion protein) and either pCAGGS-GFP or pCAGGS-GluN2B-IRES-GFP (with wild-type

or mutant mouse GluN2B). Slices were cultured for an additional 14–20 days before recording. Slices were recorded in a submersion chamber on an upright Olympus microscope, perfused in room temperature normal ACSF saturated with 95% O2/5% CO2. Picrotoxin (0.1 mM) and NBQX (10 μM) were added to the ACSF to block $GABA_A$ and AMPA receptors respectively. CA1 pyramidal cells were visualized by infrared differential interference contrast microscopy and transfected neurons were identified by epifluorescence microscopy. The intracellular solution contained (in mM) CsMeSO4 135, NaCl 8, HEPES 10, Na-GTP 0.3, Mg-ATP 4, EGTA 0.3, and QX-314 5. Cells were recorded with 3 to 5MΩ borosilicate glass pipettes, following stimulation of Schaffer collaterals with bipolar placed in stratum radiatum of the CA1 region. Series resistance was monitored and not compensated, and cells in which series resistance varied by 25% during a recording session were discarded. Synaptic responses were collected with a Multiclamp 700B amplifier (Axon Instruments, Foster City, CA), filtered at 2 kHz and digitized at 10 Hz. All paired recordings involved simultaneous whole-cell patch-clamp recordings from a transfected and neighboring untransfected neuron. EPSCs were elicited by stimulation of Schaffer collaterals with AMPAR-EPSCs recorded at −70mV and NMDAR-EPSCs recorded at +40 mV in the presence of 10 μM NBQX. The stimulus was adjusted to evoke a measurable, monosynaptic EPSC in both cells. Paired amplitude data were analyzed with a Wilcoxon signed-rank test and the paired decay kinetics were analyzed with a two-tailed paired Student's t test. Comparison of paired data groups were performed using a Mann-Whitney U test. Linear regressions were obtained using the least-squares method. All error bars represent standard error measurement.

SUPPLEMENTAL REFERENCES

Akashi, K., Kakizaki, T., Kamiya, H., Fukaya, M., Yamasaki, M., Abe, M., Natsume, R., Watanabe, M., and Sakimura, K. (2009). NMDA receptor GluN2B (GluR epsilon 2/NR2B) subunit is crucial for channel function, postsynaptic macromolecular organization, and actin cytoskeleton at hippocampal CA3 synapses. J. Neurosci. *29*, 10869–10882.

Chen, B.S., Braud, S., Badger, J.D., 2nd, Isaac, J.T., and Roche, K.W. (2006). Regulation of NR1/NR2C N-methyl-D-aspartate (NMDA) receptors by phosphorylation. J. Biol. Chem. *281*, 16583–16590.

Cousins, S.L., and Stephenson, F.A. (2012). Identification of N-methyl-D-aspartic acid (NMDA) receptor subtype-specific binding sites that mediate direct interactions with scaffold protein PSD-95. J. Biol. Chem. *287*, 13465–13476.

Elias, G.M., Funke, L., Stein, V., Grant, S.G., Bredt, D.S., and Nicoll, R.A. (2006). Synapse-specific and developmentally regulated targeting of AMPA receptors by a family of MAGUK scaffolding proteins. Neuron *52*, 307–320.

Mishina, M., and Sakimura, K. (2007). Conditional gene targeting on the pure C57BL/6 genetic background. Neurosci. Res. *58*, 105–112.

Schnell, E., Sizemore, M., Karimzadegan, S., Chen, L., Bredt, D.S., and Nicoll, R.A. (2002). Direct interactions between PSD-95 and stargazin control synaptic AMPA receptor number. Proc. Natl. Acad. Sci. USA *99*, 13902–13907.

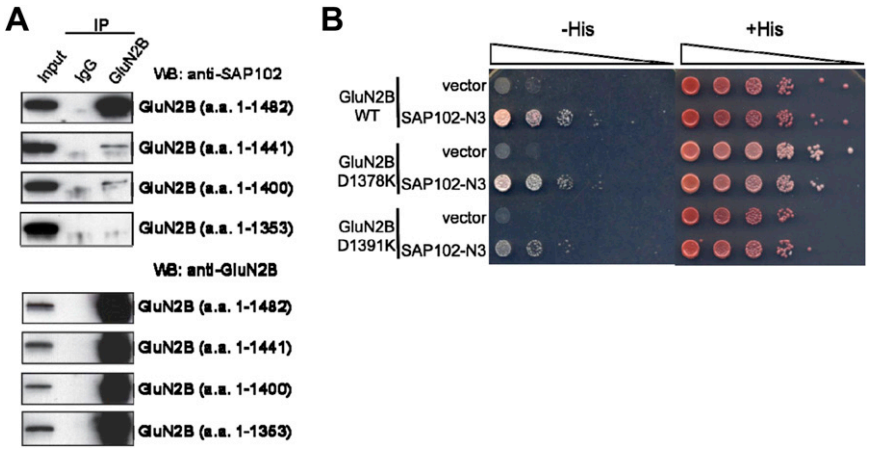

Figure S1. Characterization of the Non-PDZ Interaction between GluN2B and SAP102, Related to Figure 1

(A) Related to Figure 1A. The GluN2B (1353-1400) region is required for the PDZ-independent SAP102 binding. This figure is identical to Figure 1A(2) except that the top four panels of Figure S1 are longer exposures of top four panels of Figure 1A(2).

(B) Related to Figure 1B. GluN2B D1391K, but not D1378K, disrupts the PDZ-independent SAP102 binding. Yeast were cotransformed with LexA-GluN2B, LexA-GluN2B D1378K, or LexA-GluN2B D1391K and Gal4 vector or Gal4-SAP102-N3, and growth was evaluated on appropriate yeast selection medium. Results shown are 10-fold serial dilutions of yeast cells.

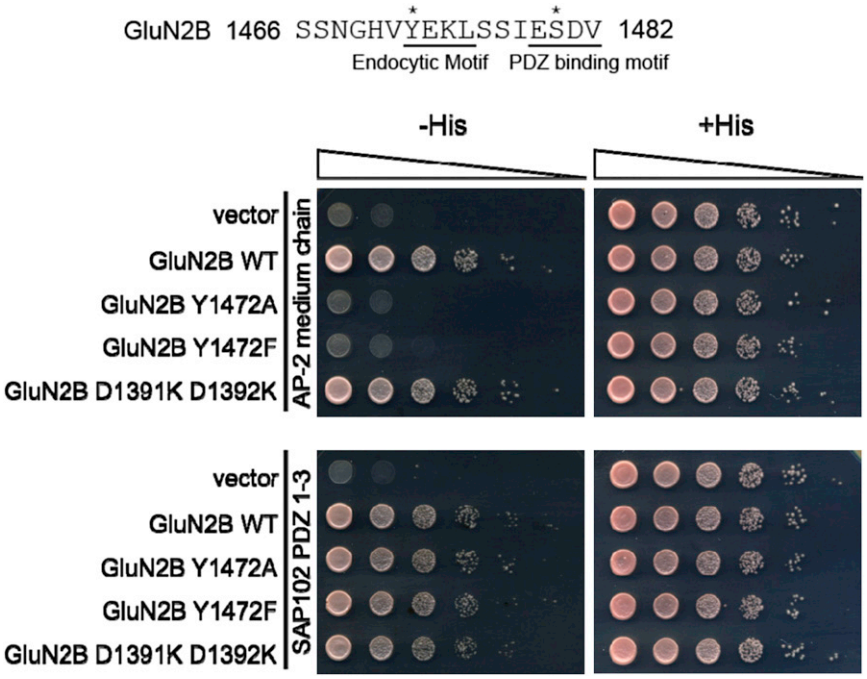

Figure S2. The GluN2B DD-KK Mutation Does Not Affect the Interaction between GluN2B and the Medium Chain (μ2) of the AP-2 Adaptor Complex, Related to Figure 2

Yeast was cotransformed with LexA-GluN2B, LexA-GluN2B Y1472A, LexA-GluN2B Y1472F, or LexA-GluN2B D1391K D1392K and Gal4-μ2 or Gal4-SAP102 (PDZ 1-3), and growth was evaluated on appropriate yeast selection medium. Results shown are 10-fold serial dilutions of yeast cells.

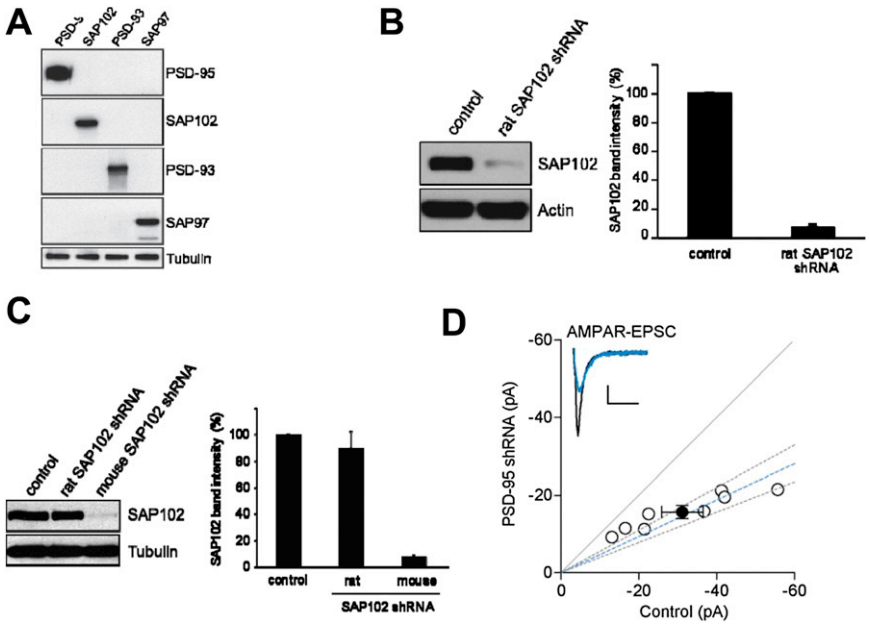

Figure S3. Characterization of Antibodies and Knockdown of SAP102 and PSD-95, Related to Figure 4

(A) HEK293 cells were transfected with PSD-95, SAP102, PSD-93 or SAP97, and immunoblots of cell lysate were probed with antibodies as indicated.

(B) Primary rat hippocampal neurons (DIV5) were infected with lentivirus expressing SAP102 shRNA or scrambled shRNA. The cell lysates were prepared at DIV13, resolved by SDS-PAGE, and immunoblotted with SAP102 or actin antibody.

(C) Primary mouse hippocampal neurons (DIV6) were infected with lentivirus containing rat SAP102 shRNA, mouse SAP102 shRNA or control shRNA. The cell lysates were prepared at DIV14, resolved by SDS-PAGE, and immunoblotted with SAP102 antibody or tubulin antibody.

(D) Cultured hippocampal slices were prepared from wild-type P7 mice, biolistically transfected with mouse PSD-95 shRNA at DIV3 and AMPAR-EPSCs were recorded at DIV8. Scatter plot represents the peak amplitudes of the AMPAR-EPSCs from single pairs (open circles) and mean ± SEM (filled circle) from transfected and control cells. Dashed lines represent linear regression and 95% confidence interval. Sample traces: control cell, black; transfected cell, blue; scale bars represent 20 ms and 5 pA. AMPAR-EPSCs were reduced to 55.0 ± 4.4% of control, consistent with previous reports in cultured hippocampal slices from rat (Elias et al., 2006).